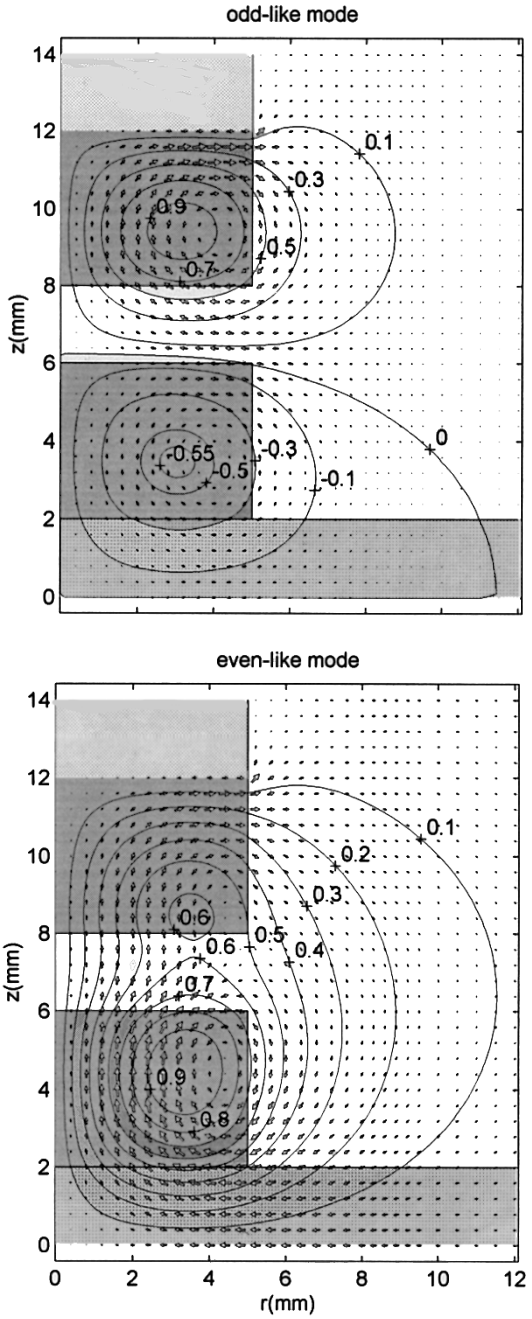

Fig. 4. Field distributions of the two $TE_{01\delta}$ modes for a double DR in a MIC environment. Normalized contour lines for field E_ϕ and flux lines for fields H_r and H_z.

MIC's are also shown probably for the first time. These results are helpful in the design of DR oscillators and filters.

REFERENCES

[1] E. Marchionna, E. Martini, and A. Panzeri, "Dielectric resonator wide band tuning cavity for high performance filters," in *Proc. 17th European Microwave Conf.*, 1987, pp. 865–871.

[2] R. K. Mongia and P. Bhartia, "Accurate conductor Q-factor of dielectric resonator placed in an MIC environment," *IEEE Trans. Microwave Theory Tech.*, vol. 41, pp. 445–449, Mar. 1993.

[3] M. Jaworski and M. W. Pospieszalski, "An accurate solution of the cylindrical dielectric resonator problem," *IEEE Trans. Microwave Theory Tech.*, vol. MTT-27, pp. 639–643, July 1979.

[4] S. Maj and J. W. Modelski, "Application of a dielectric resonator on microstrip line for a measurement of complex permittivity," in *1984 IEEE MTT-S Int. Microwave Symp. Dig.*, pp. 525–527.

[5] S. Maj, A. Abramowicz, and J. Modelski, "Computer-aided design of mechanical tuning structures of a dielectric resonator on microstrip substrate," in *Proc. 17th European Microwave Conf.*, 1987, pp. 859–864.

[6] Y. Kobayashi, T. Aoki, and Y. Kabe, "Influence of conductor shields on the Q-factors of a TE_0 dielectric resonator," *IEEE Trans. Microwave Theory Tech.*, vol. MTT-33, pp. 1361–1366, Dec. 1985.

[7] M. Yousefi, S. K. Chaudhuri, and S. Safavi-Naeini, "GIBC formulation for the resonant frequencies and field distribution of a substrate-mounted dielectric resonator," *IEEE Trans. Antennas Propagat.*, vol. 42, pp. 38–46, Jan. 1994.

[8] F. H. Gil and J. P. Martinez, "Analysis of dielectric resonators with tuning screw and supporting structure," *IEEE Trans. Microwave Theory Tech.*, vol. MTT-33, pp. 1453–1457, Dec. 1985.

[9] C. C. Su and J. M. Guan, "Finite-difference analysis of dielectric-loaded cavities using the simultaneous iteration of the power method with the Chebyshev acceleration technique," *IEEE Trans. Microwave Theory Tech.*, vol. 42, pp. 1998–2006, Oct. 1994.

[10] M. Mohammad-Taheri and D. Mirshekar-Syahkal, "Computation of Q-factors of dielectric-loaded cylindrical cavity resonators," *Proc. Inst. Elect. Eng.*, vol. 137, pt. H, pp. 372–376, Dec. 1990.

[11] S. Fiedziuszko and A. Jelenski, "Double dielectric resonator," *IEEE Trans. Microwave Theory Tech.*, vol. MTT-19, pp. 779–781, Sept. 1971.

[12] K. Wada, E. Nagata, and I. Haga, "Wideband tunable DR VCO," in *Proc. 15th European Microwave Conf.*, 1985, pp. 407–412.

A Waveguide-to-Microstrip Transition with a DC/IF Return Path and an Offset Probe

S. C. Shi and J. Inatani

***Abstract*— This paper describes a type of waveguide-to-microstrip transition incorporated with a "built-in" DC/IF return and an offset probe which is proposed for the applications of submillimeter-wave superconducter–insulator–superconductor (SIS) mixers. The effects of the DC/IF return and the probe location and orientation are understood by simulating a 100-GHz transition using the finite element method (FEM). The simulation results are compared to the experimental results of a Ka-band scale model for the simulated transition. The performance of a 100-GHz SIS mixer employing such a transition is finally presented.**

***Index Terms*—Probe, SIS mixer, waveguide transition.**

I. INTRODUCTION

Conventional waveguide superconducter–insulator–superconductor (SIS) mixers, which employ one or two mechanical tuners to adjust the mixer's RF impedance to suit the SIS junction (or array of junctions), are inappropriate to complex systems such as a focal-plane receiver array or an interferometer array and are not desirable for single receivers due to the inconvenience of operating. It is, therefore, important to develop tuneless SIS mixers. To yield a tuneless waveguide SIS mixer, broadband RF matching between the

Manuscript received June 16, 1995; revised November 21, 1996.

The authors are with the Nobeyama Radio Observatory, National Astronomical Observatory of Japan, Nobeyama, Nagano, 384-13 Japan.

Publisher Item Identifier S 0018-9480(97)01720-1.

0018–9480/97$10.00 © 1997 IEEE

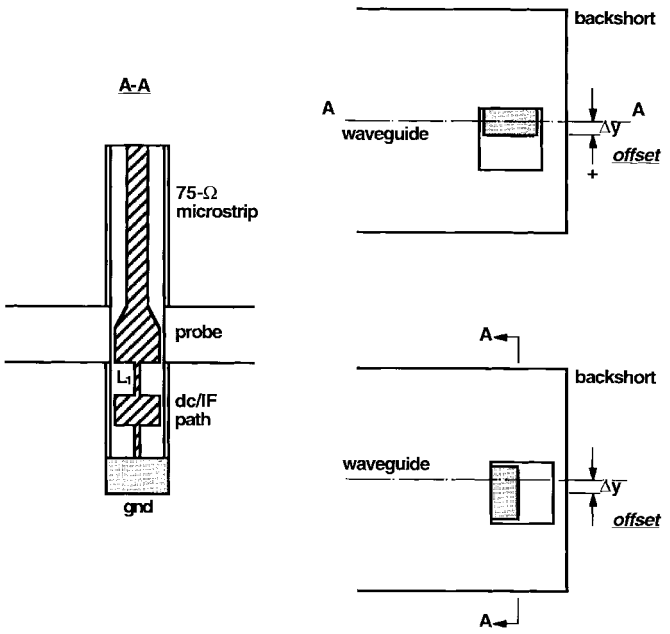

Fig. 1. Cross-sectional views of the proposed waveguide-to-microstrip transition, with the substrate structure (left) and two different substrate configurations, parallel (upper right) and perpendicular (lower right) to the waveguide E-plane.

TABLE I
DIMENSIONAL PARAMETERS (UNITS ARE IN MM) OF THE 100-GHZ WAVEGUIDE-TO-MICROSTRIP TRANSITION

waveguide	2.54 x 0.635
WG aperture	0.7 x 0.7
substrate	0.6 x 0.3
probe	0.5 x 0.385 + taper x 0.25
75-ohm MS	W0 = 0.235
DC/IF return	W1 = 0.06, L1 = 0.375
	W2 = 0.50, L2 = 0.340
	W3 = 0.06, L3 = 0.375
probe offset*	0.3
backshort length*	0.625 (*Para. Probe*)
	0.550 (*Perp. Probe*)

* *optimized* unit: mm

input waveguide (of a characteristic impedance around 500 Ω) and the SIS junction (of a typical input impedance less than 100 Ω) is essential. A very reduced-height waveguide is quite effective but may become too small-sized to be fabricated in the short millimeter- and submillimeter-wave regimes. A waveguide-to-microstrip transition might be a good alternative, while one intends to place the SIS junction on a microstrip line other than in the waveguide. It is well known, however, that traditional waveguide-to-microstrip transitions [1] lack a DC/IF return which cannot be excluded in mixers. Although one may realize this return path just by simply connecting a quarter-wavelength high-impedance line from the microstrip line to the ground [2], it is inconvenient to make such an arrangement and difficult to control its length especially at submillimeter wavelengths. Thus, in this paper, the authors propose a type of waveguide-to-microstrip transition including a "built-in" DC/IF return.

II. SIMULATION AND DESIGN

A. Structure

As is illustrated in Fig. 1, the proposed waveguide-to-microstrip transition (with two different substrate orientations) is made up of an input waveguide, a tuning waveguide backshort, a microstrip line in a metallic enclosure, a strip probe, and a DC/IF return. Linking the main microstrip and the DC/IF return, the strip probe is as long as the waveguide height. Because a long probe is not useful for broadband transitions [3], the authors considered only the case of a half-reduced height waveguide. Such a waveguide indeed makes it easier to match the microstrip line because of a smaller waveguide impedance (around 234 Ω at 100 GHz), and may be connected either to a standard waveguide through a tapered waveguide transition or directly to a specially designed feed horn. The impedance seen at the microstrip port was assumed to be 75 Ω, namely the characteristic impedance of the microstrip line.

For this type of transition, a small aperture in the broad wall of the waveguide is certainly useful in minimizing its effect upon the field distribution in the waveguide so as to ensure the design accuracy. In contrast, SIS mixers prefer a large substrate chip for handling and mounting, especially at submillimeter wavelengths. Thus, the aperture should be taken as large as possible, so long as it is capable of suppressing all the waveguide modes there. In this paper, the authors took an example of this type of transition at 100 GHz. Assuming a 0.6-mm wide and 0.3-mm thick quartz substrate ($\varepsilon_r = 3.8$) for this 100-GHz transition, the authors chose an aperture measuring 0.7 mm × 0.7 mm. The corresponding cutoff frequency of waveguide modes is around 177 GHz, which is far beyond the operation frequencies of the 100-GHz transition.

Although the input impedance seen at the microstrip port is generally independent upon the probe width, a narrow probe might limit the transition's matching bandwidth and result in an excessive inductance loss [1]. Thus, a 0.5-mm wide probe connecting to the main microstrip via a short section of taper was adopted. The DC/IF return, i.e., the circuit connected at the end of the probe, consists of two sections of high-impedance line (126.9 Ω) and one section of low-impedance line (44.8 Ω) whose lengths are initially determined so that a perfect open circuit can be seen at the end of the probe at 100 GHz. All the dimensional parameters of the 100-GHz transition are summarized in Table I.

B. Simulation

The finite element method (FEM) should be effective in simulating this waveguide-to-microstrip transition as far as its structure is concerned. If the DC/IF return and the probe location are fixed there would be only one free parameter, namely the backshort position, remaining to be determined. Nonetheless, it still must be very time consuming to utilize a FEM simulator like a high-frequency structure simulator (HFSS) [4] to simulate this transition in a "zigzag" manner. Thus, in this paper the authors adopted a simulation scheme as proposed in [3], that is firstly to employ HFSS to evaluate the S-parameters of a three-port structure (i.e., the transition with its backshort removed) and then to use those S-parameters to compute the reflection coefficient at the microstrip port for the instance of the two waveguide ports terminated by a matching load and a length-varying backshort, respectively. The optimum backshort position is determined so that the calculated reflection coefficients are minimized in the frequency range of interest.

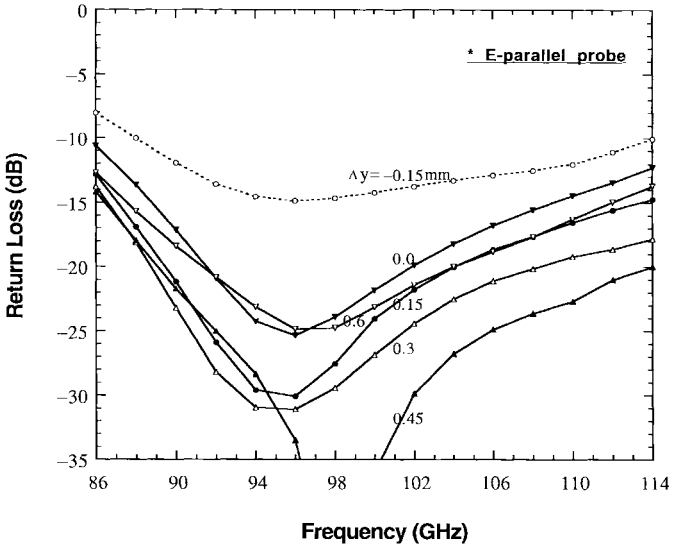

Fig. 2. Simulated return loss at the microstrip port of the 100-GHz waveguide-to-microstrip transition with an E-plane-parallel substrate orientation, plotted as functions of frequency and the probe offset. The optimized backshort lengths corresponding to different probe offsets are 0.475 (-0.15), 0.55 (0.0), 0.575 (0.15), 0.625 (0.3), 0.675 (0.45), and 0.725 (0.6) mm, respectively.

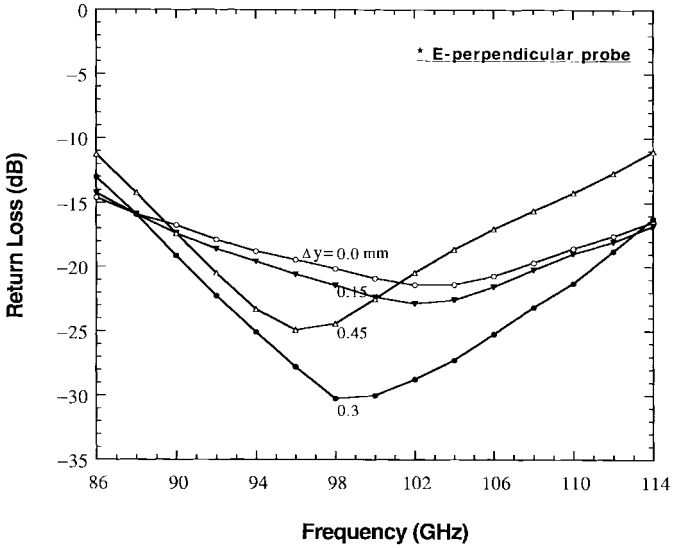

Fig. 3. Simulated return loss at the microstrip port of the 100-GHz waveguide-to-microstrip transition with an E-plane-perpendicular substrate orientation, plotted as functions of frequency and the probe offset. The optimum backshort lengths are the same, about 0.55 mm from the substrate surface, for all different probe offsets.

Firstly, the authors investigated this 100-GHz transition for such a configuration that the strip probe is located in the central waveguide E-plane as common treatments (i.e., offset $\Delta y = 0$, see Fig. 1). Prior to finding out its optimum backshort position, the effect of the DC/IF return was examined. The authors have simulated this transition for several instances in relation to different lengths (L_1) of the first section of the DC/IF return. Notice that the other two sections of the DC/IF return were fixed at 0.34 and 0.375 mm, respectively, providing a perfect short circuit at the end of the first section at 100 GHz. It has been found that the instance of $L_1 = 0.375$ mm presents the most satisfactory frequency characteristic for the transition. However, the input reflection coefficient of the DC/IF return at 100 GHz, calculated for the case of $L_1 = 0.375$ mm, was not a perfect open circuit as expected, instead of 1/40°. This discrepancy is probably due to the effect of the discontinuity between the probe and the DC/IF return. Furthermore, the matching bandwidth of the transition was found still quite limited even with an optimized backshort position (see Fig. 2). Besides the two relatively large apertures, the long strip probe (possibly of a large inductance) was thought of as the main cause of a limited bandwidth. As the probe length was already fixed, the authors sought to improve the transition's matching bandwidth by offsetting the strip probe a distance (Δy) from the central E-plane, which might similarly alter the effective inductance of the probe. This transition has been simulated for a number of cases related to different probe offsets. It should be pointed out that the aperture location was changed to suit the probe shift and that the DC/IF return was fixed at $L_1 = 0.375$ mm and the backshort position was optimized for each case. The simulation results are plotted in Fig. 2. Clearly, there is a probe offset (i.e., $\Delta y = 0.3$ or 0.45 mm) of which the transition has the largest bandwidth. Additionally the larger the probe offset, the longer the backshort position is.

It is also of particular interest to investigate another configuration of the transition, i.e., having the strip probe perpendicular to the E-plane (see Fig. 1), as such a configuration can ease the fabrication of tuneless waveguide mixer mounts. Unlike the one investigated just before, this configuration has a symmetrical structure so that it is necessary to study only the case of the strip probe shifted toward one direction. The 100-GHz transition with this configuration has also been simulated for different probe offsets. Note that the DC/IF return was kept the same as in the previous configuration. Similarly, the transition bandwidth was improved by offsetting the probe, as can be seen from Fig. 3. The optimum probe offset Δy was found to be also around 0.3 mm, but the optimum backshort position (0.55 mm from the surface of the substrate) was hardly influenced with the variation of the probe location.

III. Experiment

A. Ka-Band Waveguide-to-Stripline Transition

It is appropriate to verify the simulation accuracy and reliability by comparing the simulated and experimental results. A Ka-band scale model for the 100-GHz waveguide-to-microstrip transition, which is associated with an E-plane-paralleled and 0.3-mm offset probe, has been fabricated. The scaling factor was taken as fourteen so that the scaled waveguide was measuring 7.11 mm × 1.78 mm. Both the lengths of the first section of the DC/IF return and of the backshort were scaled in accordance with their optimum values of 0.375 and 0.625 mm, respectively. For the sake of convenience of performing experiments, two scaled transitions were connected back-to-back with a separation of 11-mm long microstrip line built on a 0.84-mm thick quartz substrate, as displayed in Fig. 4. Two waveguide tapers (full- to half-height) were also included in this test device to meet the measurement system. Using an HP8757 scalar network analyzer, the authors have measured the performance of the test device. As demonstrated in Fig. 5, the return loss is apparently less than -15 dB in the frequency range of 31–42 GHz (of a 30% relative bandwidth), and the insertion loss is only about 0.5 dB including losses arising from the microstrip line, input and output waveguides, and two waveguide taper transitions. The insertion loss of a single transition is approximately 0.1 dB, if taking into account the losses due to the two waveguide taper transitions (0.15 dB, measured) and the

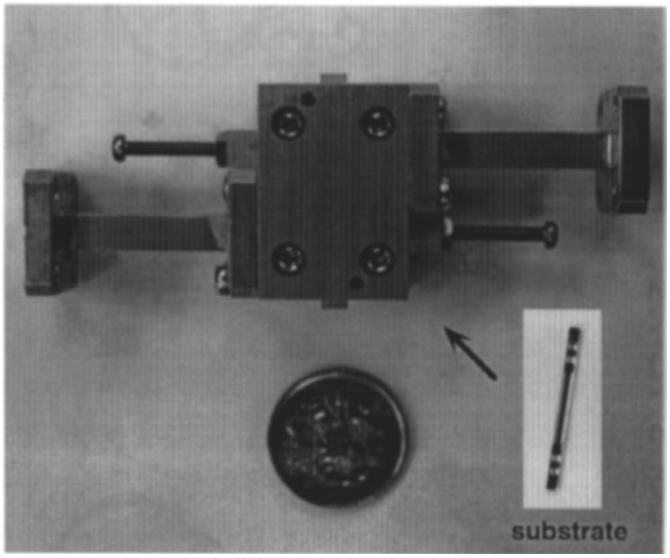

Fig. 4. Photograph of a Ka-band test device made up of two scaled transitions connected back-to-back and separated by an 11-mm long microstrip line. Note that two waveguide taper (from full- to half-height) transitions are also included.

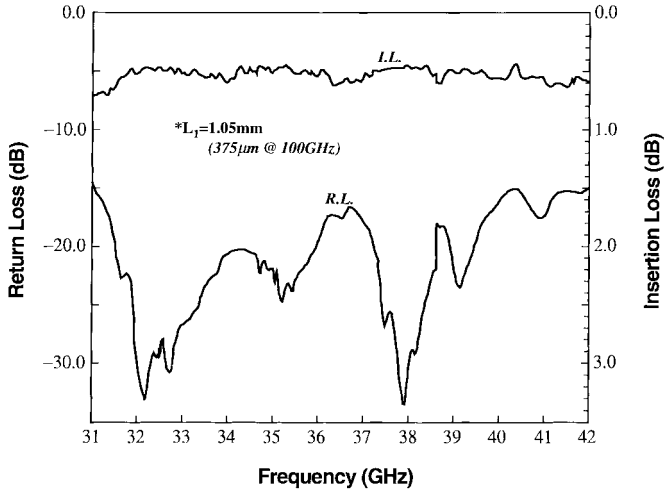

Fig. 5. Measured insertion and return losses of the Ka-band test device, as a function of frequency.

microstrip line (0.15 dB, calculated) and assuming a symmetrical structure.

B. 100-GHz SIS Mixer

A 100-GHz tuneless SIS mixer employing such a waveguide-to-microstrip transition has been developed [5]. The input impedance of the SIS junction is around 10 Ω, which is matched to a half-reduced-height waveguide through the waveguide-to-microstrip transition and two sections of quarter-wavelength impedance transformer integrated in the junction chip. The noise performance of this SIS mixer is exhibited in Fig. 6. Apparently, the double sideband (DSB) noise temperature of the overall receiver system, which is composed of a vacuum window at room temperature, an IR filter at 77 K, the 100-GHz SIS mixer at 4-K level, and an L-band FET amplifier at about 20 K, is less than 40 K over the frequency range of 80–120 GHz. The best published results for tunable waveguide SIS mixers [6], [7] at this frequency band are also shown in Fig. 6. Clearly, the authors' results are comparable or superior.

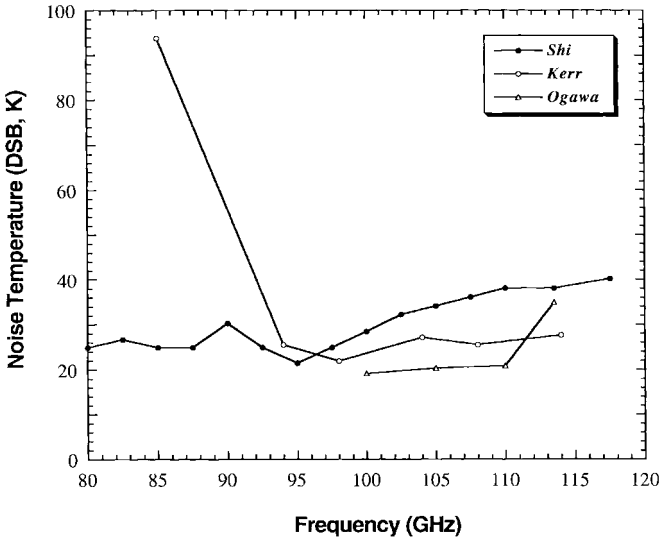

Fig. 6. Overall receiver noise performance for the 100-GHz SIS mixer incorporating a waveguide-to-microstrip transition.

IV. Conclusion

A type of waveguide-to-microstrip transition featuring an offset probe and a "built-in" DC/IF return has been extensively investigated. It has been found that the DC/IF return should provide an open circuit at the probe's end to minimize its effect upon the transition bandwidth and that the bandwidth can be improved considerably by offsetting the probe to a certain position (for two different substrate orientations). Both the simulation and scaling experimental results have demonstrated that this type of transition has a very low insertion loss ($<$0.1 dB) over a 30% relative bandwidth. Excellent performance by a 100-GHz SIS mixer proves that this type of transition is rather broadband. It should find its use in millimeter- and submillimeter-wave components.

Acknowledgment

The authors wish to thank K. Miyazawa and H. Iwashita for their assistance in securing measurement equipment and are also grateful to T. Noguchi for helpful discussions.

References

[1] Y. C. Shih, T. N. Ton, and L. Q. Bui, "Waveguide-to-microstrip transitions for millimeter-wave applications," in *IEEE MTT-S Dig.*, New York, May 1988, pp. 473–475.

[2] A. R. Kerr, S.-K. Pan, S. Whiteley, M. Radparvar, and S. Faris, "A fully integrated SIS mixer for 75–110 GHz," in *IEEE Int. Microwave Symp. Dig.*, Dallas, TX, May 1990, pp. 851–854.

[3] S. C. Shi and J. Inatani, "A 330–390 GHz waveguide-to-suspended stripline transition," in *Proc. 3rd Int. Conf. on Millimeter-Wave and Far-IR Sci. and Tech.*, Gail M. Tucker, Ed. Guangzhou, China, Aug. 1994, pp. 219–222.

[4] Hewlett-Packard Co., Network Measurements Div., Santa Rosa, CA 95403.

[5] S. C. Shi, T. Noguchi, and J. Inatani, "A fixed-tuned SIS mixer exhibiting broad bandwidth and very low noise temperature," in *Extended Abstracts 5th Int. Supercond. Electron. Conf. (ISEC'95)*, Nagoya, Japan, July 1995, pp. 410–412.

[6] A. R. Kerr and S.-K. Pan, "Some recent developments in the design of SIS mixers," *Int. J. Infrared Millim. Waves*, vol. 11, no. 10, pp. 1169–1187, Oct. 1990.
[7] H. Ogawa, A. Mizuno, M. Moko, H. Ishikawa, and Y. Fukui, "A 110 GHz SIS receiver for radio astronomy," *Int. J. Infrared Millim. Waves*, vol. 11, no. 6, pp. 717–726, June 1990.

Analysis of General Lossy Inhomogeneous and Anisotropic Waveguides by the Finite-Element Method (FEM) Using Edge Elements

Luis Nuño, Juan V. Balbastre, Héctor Castañé

***Abstract*—Several finite element formulations based on edge elements have been developed in recent years, avoiding the appearance of spurious modes in waveguides. However, no formulation of this kind dealing with general lossy inhomogeneous and anisotropic waveguides has been found in the literature. In this paper, a new finite element scheme for the most general linear waveguides has been derived from vector wave equations via a Galerkin procedure. In this formulation, triangular and quadrilateral edge elements have been used in order to avoid the spurious solutions. Furthermore, the final eigensystem involves only very sparse matrices, thus allowing important savings in time and memory.**

***Index Terms*— Anisotropic waveguides, edge elements, finite-element method.**

I. Introduction

The finite-element method (FEM) has been widely used in electromagnetics for the last two decades. Nevertheless, the earlier finite element analyses had the drawback of the appearance of spurious modes, leading to a considerable effort to avoid such nonphysical solutions [1]–[6].

More recently, two conditions have been found as requirements to avoid spurious solutions [7]: compatibility to guarantee the continuity of the tangential components of the fields and unisolvence to correctly model the curl operator null-space.

In the last years, several finite element formulations using vectorial interpolation have been developed [8]–[12]. Those vectorial elements satisfy both compatibility and unisolvence conditions so they do not present spurious modes. However, in the formulations of this kind found in the literature only lossless diagonal anisotropic waveguides have been considered. In this paper, the authors present a new edge element formulation valid for the most general lossy inhomogeneous and anisotropic linear waveguides.

First, a weak formulation of vector wave equations is obtained. This integral equation is valid for general anisotropic waveguides bounded by perfect electric or magnetic walls. Then, this integral equation is discretized following the FEM, obtaining a very sparse eigensystem where the eigenvalue is the propagation constant, attaining an important reduction in memory and central processing unit (CPU) time.

Manuscript received August 22, 1995; revised November 21, 1996. This work was supported by the Spanish CICYT, TIC95-0983-C03-02.

The authors are with the Departamento dé Comunicaciones, E.T.S.I. Telecomunicación de Valencia, Universidad Politécnica de Valencia, 46071, Valencia, Spain.

Publisher Item Identifier S 0018-9480(97)01718-3.

II. Weak Formulation

For the most general case of waveguides filled with lossy inhomogeneous and anisotropic materials, the problem is governed by the following vector wave equations:

$$\nabla \times (\hat{\mu}_r^{-1} \nabla \times \vec{E}) - k_0^2 \hat{\varepsilon}_r \vec{E} = 0$$
$$\nabla \times (\hat{\varepsilon}_r^{-1} \nabla \times \vec{H}) - k_0^2 \hat{\mu}_r \vec{H} = 0, \qquad k_0^2 = \omega^2 \varepsilon_0 \mu_0 \tag{1}$$

where $\hat{\varepsilon}_r$ and $\hat{\mu}_r$ are the relative electric permittivity and magnetic permeability tensors, respectively,

$$\hat{\varepsilon}_r = \begin{bmatrix} \varepsilon_{xx} & \varepsilon_{xy} & \varepsilon_{xz} \\ \varepsilon_{yx} & \varepsilon_{yy} & \varepsilon_{yz} \\ \varepsilon_{zx} & \varepsilon_{zy} & \varepsilon_{zz} \end{bmatrix}$$
$$\hat{\mu}_r = \begin{bmatrix} \mu_{xx} & \mu_{xy} & \mu_{xz} \\ \mu_{yx} & \mu_{yy} & \mu_{yz} \\ \mu_{zx} & \mu_{zy} & \mu_{zz} \end{bmatrix}. \tag{2}$$

The boundary conditions for electric or magnetic walls are, respectively,

$$\hat{n} \times \vec{E}|_C = 0$$

or

$$\hat{n} \times \vec{H}|_C = 0. \tag{3}$$

Assuming an exponential dependence of the fields with the z coordinate

$$\vec{E} = \vec{E}_0(x, y) e^{-\gamma z}$$
$$\vec{H} = \vec{H}_0(x, y) e^{-\gamma z}, \qquad \gamma = \alpha + j\beta \tag{4}$$

and defining the differential operators

$$D = \frac{\partial}{\partial x}\hat{x} + \frac{\partial}{\partial y}\hat{y} - \gamma \hat{z}$$
$$\overline{D} = \frac{\partial}{\partial x}\hat{x} + \frac{\partial}{\partial y}\hat{y} + \gamma \hat{z} \tag{5}$$

leads to very elegant and compact expressions after applying the Galerkin procedure to the waveguide section S:

$$\iint_S (\overline{D} \times \vec{F}_0) \cdot (\hat{\mu}_r^{-1} D \times \vec{E}_0)\, dS - k_0^2 \iint_S \vec{F}_0 \cdot (\hat{\varepsilon}_r \vec{E}_0)\, dS = 0 \tag{6a}$$

$$\iint_S (\overline{D} \times \vec{G}_0) \cdot (\hat{\varepsilon}_r^{-1} D \times \vec{H}_0)\, dS - k_0^2 \iint_S \vec{G}_0 \cdot (\hat{\mu}_r \vec{H}_0)\, dS = 0 \tag{6b}$$

with $\vec{F}_0$ and $\vec{G}_0$ being the test functions, which satisfy the same boundary conditions as $\vec{E}_0$ and $\vec{H}_0$, respectively.

III. Finite Element Scheme

Because of the dual form of (6), only the finite element scheme for the electric field derived from (6a) will be presented. The transversal components of $\vec{E}_0$ and $\vec{F}_0$ will be interpolated with the first-order vector edge functions while their axial components will be

0018–9480/97$10.00 © 1997 IEEE